ADVANCED FUNCTIONAL MATERIALS
www.afm-journal.de

Confinement Leads to Control over Calcium Sulfate Polymorph

*Yun-Wei Wang, Hugo K. Christenson, and Fiona C. Meldrum**

Although many processes of great biological, technological, and environmental importance, such as the formation of biominerals, the templating of nanostructures, and salt weathering, occur in confinement rather than in bulk solution, little is known about the influence of confinement over the precipitation of inorganic crystals. The effects of confinement on the precipitation of calcium sulfate are investigated using a crossed-cylinder apparatus which offers confinement that varies continuously from zero to tens of micrometers. While the thermodynamically stable form of calcium sulfate (gypsum) is always observed at large surface separations, a remarkable stabilization of the metastable phases amorphous calcium sulfate (ACS) and calcium sulfate hemihydrate (bassanite, plaster of Paris) is observed even at micrometer-scale separations. For the first time, the approach is extended to study the combined effects of soluble additives and confinement, which are often present in natural or synthetic systems, and it is shown that this considerably extends the lifetimes of ACS and hemihydrate. These confinement effects are attributed to hindered aggregation of precursor particles at small surface separations, which limits polymorph conversion. While these results have immediate relevance to salt weathering and biomineralization processes, they are also important to the many crystallization and aggregation-driven processes occurring in small volumes.

1. Introduction

Many important phenomena as varied as the production of nanomaterials, pharmaceuticals and food stuffs, weathering and frost heave, ice formation in the atmosphere and the generation of biominerals such as seashells are based on crystallization. The ability to effectively control crystallization processes therefore promises to optimize products and synthetic methods, to minimize undesirable processes such as scale deposition or kidney stone formation and to achieve repair over structures such as bones and teeth. The most widespread control strategy employed is undoubtedly the use of soluble additives, where these can selectively affect nucleation and growth processes, leading to changes in particle numbers and sizes as well as morphology and polymorph, or even inhibition of crystal growth.[1–4] There is, however, strong evidence that the physical environment in which a crystal forms can also lead to control over many features such as morphology, size, orientation and polymorph.[5,6] Indeed, although experiments attempting to control crystallization are usually carried out in bulk solution, many processes, such as biomineralization and weathering, actually occur within small volumes, where the confining surfaces become increasingly important in defining the product material.[7–11]

The effects of confinement on crystallization have been investigated since early last century, when the first studies addressed crystallization of liquids in porous solids. Subsequently, with the increasing availability of better-defined porous media, thousands of studies have been carried out on crystallization in confinement. However, almost all the work has dealt with the freezing of pure liquids, e.g. water, hydrogen, inert gases, organic liquids and metals, where a depression of the freezing and melting points is observed with a reduction in the sizes of nanopores.[6,12] By comparison, only a handful of studies have systematically investigated the effects of confinement on crystallization from solution, and virtually all of these are relatively recent reports of the formation of organic/molecular crystals.[5,13–15] There has been next to no work on the crystallization of inorganic substances in confinement, despite the central importance of such compounds in materials science.

There is, however, good evidence that confinement can influence crystallization from solution on many levels. Where unlimited growth is undesirable, confinement provides an effective route to controlling crystal size and shape.[9] Indeed, this forms the basis of templating approaches where the product crystal can adopt complex morphologies imposed by the confining volume.[16–18] Confinement also affects the nucleation/early stages of growth and can thus influence crystal orientation, polymorph and polycrystallinity. When preferential orientation occurs in an anisotropic growth environment (e.g., a cylindrical pore), it is usually observed that the axis corresponding to the fastest growth direction is aligned with the axis of the pore.[19–22] Precipitation within small volumes can also lead to stabilization of metastable crystal polymorphs and amorphous phases due to critical size or kinetic effects.[5,13,23–31] Finally, as

Y.-W. Wang, Prof. F. Meldrum
School of Chemistry
Woodhouse Lane, Leeds, LS2 9JT, UK
E-mail: F.Meldrum@leeds.ac.uk
Dr. H. K. Christenson
School of Physics and Astronomy
Leeds, LS2 9JT, UK

DOI: 10.1002/adfm.201300861

a constrained reaction volume offers an environment in which nuclei are maintained in proximity to each other, competitive growth can dictate whether the product is a single crystal or polycrystalline in structure.[32–35]

Here, we address this issue and perform a systematic investigation of the effects of confinement on the precipitation of an inorganic crystal –calcium sulfate - which with its polymorphic character and widespread use, provides an excellent candidate for our study. Further, recent studies on the mechanism of calcium sulfate precipitation from aqueous solution have drawn new attention to this material by identifying for the first time a short-lived amorphous calcium sulfate (ACS) phase[36] and demonstrating that calcium sulfate dihydrate (gypsum) can form via ACS and calcium sulfate hemihydrate (bassanite, $CaSO_4 \cdot 0.5H_2O$) phases.[36–38] We then extend the work to investigate for the first time the combined effects of both confinement and soluble additives on crystallization– both of which are present in many natural/synthetic systems. Our results demonstrate a systematic stabilization of increasingly metastable phases with greater degrees of confinement, and show that remarkable stabilization can be achieved when additives are also present. The work suggests that confinement provides a novel way of identifying short-lived intermediary phases, and is also of significance to salt weathering[7] and biomineralization processes, both of which occur in confinement.

2. Experimental Methods

The effects of confinement were studied by precipitating $CaSO_4$ from supersaturated aqueous solution in the annular wedge created between two crossed half-cylinders of glass and comparing particle sizes, morphologies and polymorphs with precipitates obtained in bulk solution. The combined effects of confinement and soluble additives were also investigated by adding poly(acrylic acid) (PAA) and sodium triphosphate to the reaction solutions. All data presented are fully representative of the entire crystal populations.

2.1. Precipitation of Calcium Sulfate in Confinement

Glass tubes with diameters of 25 mm were cut into 25 mm long half-cylinders. The half-cylinders were cleaned by overnight immersion in Piranha solution (sulfuric acid:hydrogen peroxide = 3:1), followed by thorough rinsing with Millipore water (18.2 MΩ), ethanol and finally drying with nitrogen gas. The half-cylinders were then mounted in a Teflon holder such that the curved surfaces faced each other with orthogonal cylinder axes. Metal screws on the top of the holder acting against a helical spring provided a slowly increasing force to gently bring the glass surfaces into contact. The surface separation, *SS*, between two crossed cylinders of equal radius of curvature, *R*, is equivalent to that of a sphere of the same radius, *R*, on a flat surface. It is related to the radial distance the contact point, *DCP*, by:

$$SS = R - \sqrt{R^2 - (DCP)^2} \approx (DCP)^2/2R \quad (1)$$

SS varies continuously from zero at the contact point, to 2–3 mm at the vapor interface of the solution droplet.[29] 200 mM solutions of $CaCl_2$ and Na_2SO_4 were prepared by dissolving $CaCl_2 \cdot 2H_2O$ and Na_2SO_4 (Sigma-Aldrich) in ultrapure Millipore water (18 MΩ/cm) respectively, and a 100 mM supersaturated solution of $CaSO_4$ was prepared by combining equal volumes of these. A 20 μL volume of this metastable $CaSO_4$ solution was then injected around the contact point of the two crossed cylinders and the holder was placed in a desiccator with open vessels of water to maintain the humidity at close to 100% to minimize evaporation. Precipitation was allowed to proceed for 1 to 30 h before being terminated by flushing the system with ethanol while the surfaces were still in contact.

Some experiments were also performed with a carbon-coated Cu transmission electron microscopy (TEM) grid placed between the two crossed cylinders at their contact point. In this case the surface separation corresponding to a particular *DCP* is approximately *SS*/2. At the end of the experiment the reaction was again terminated by flushing with ethanol, and filter paper was used to draw off excess solvent. The half-cylinders were then slowly separated. Some TEM grids supporting calcium sulfate precipitates were heated to 200 °C for 10 h prior to examination in the TEM to aid polymorph identification. Experiments were also performed in order to investigate the combined influence of confinement and additives on calcium sulfate precipitation. Here, poly(acrylic acid) (PAA, MW 8000) or sodium triphosphate (Sigma-Aldrich) were introduced into the supersaturated $CaSO_4$ solution at concentrations of 100 μg/mL and 10 μg/mL, respectively, prior to introduction of the reaction solution into the crossed-cylinder apparatus.

2.2. Characterization of Calcium Sulfate Precipitated in Confinement

The precipitates were imaged with scanning electron microscopy (SEM) and TEM, and elemental composition and polymorph were determined using energy-dispersive X-ray analysis (EDX) and electron diffraction respectively. For SEM, glass cylinders supporting calcium sulfate particles were mounted on SEM stubs using conducting carbon tape, and then sputter-coated with a 5 nm layer of Pt. All samples were examined using a Phillips XL–30 ESEM or a Leo 5000-SEM operating at 3 kV. TEM studies were performed of calcium sulfate precipitates deposited on the TEM grids inserted between the crossed cylinders and analysis was performed using a Phillips Tecnai FEG-TEM operating at 200 kV.

2.3. Control Experiments: Precipitation of Calcium Sulfate in Bulk Solution

Control experiments were performed where calcium sulfate was precipitated in bulk solution. Aqueous solutions of 200 mM $CaCl_2 \cdot 2H_2O$ and Na_2SO_4 were combined in a crystallization dish under stirring to give a final concentration of 100 mM $CaSO_4$. Glass slides were placed at the base of the dish and crystallization was allowed to proceed from unstirred solutions. For experiments carried out in the presence of the additives PAA

and sodium triphosphate, these were introduced into the sulfate solution prior to mixing with the calcium solution. These bulk precipitates were then isolated by filtration through a 0.2 μm filter membrane, washing with ethanol and air-drying and characterization was performed using a range of techniques. The shapes and sizes of the particles were determined using SEM and TEM while electron diffraction, Raman microscopy, infrared spectroscopy and powder X-ray diffraction (XRD) were used to determine polymorphs. Raman microscopy was carried out using a Renishaw 2000 Raman microscope operating with a 785 nm diode laser, while infrared spectroscopy was carried out using a Perkin Elmer Spectrum 100 Fourier transform infrared (FTIR) fitted with a diamond attenuated total reflectance (ATR) element. XRD data were collected between 10° and 60° in intervals of 0.02° and a scan rate of 0.05°/min using a Bruker D8 diffractometer with CuKα_1 radiation and a Lynx eye detector.

3. Results

In bulk solution, gypsum was the sole product from 100 mM $CaSO_4$ solutions after a reaction time of 1 h. The crystals of gypsum were single needles/plates, or clusters of intergrown needles, up to several micrometers in length (**Figure 1**a), and the polymorph was confirmed using XRD and Raman microscopy, where the peaks at 419 cm^{-1} (ν_2) and 1139 cm^{-1} (ν_3) identified the dihydrate phase (Figure S1, Supporting Information).[39] It is noted that the different phases of calcium sulfate are strictly pseudo-polymorphs due their different levels of hydration, but the widely adopted term polymorph will be used here, for simplicity. The evolution of these crystals was also studied by sampling the reaction solution over time. 200 to 300 nm blocky nanorods of calcium sulfate hemihydrate were isolated after 1 min (Figure 1b), the shortest time at which precipitates could be isolated, as confirmed by XRD and Raman microscopy (Figure S2, Supporting Information), where the peak at 435 cm^{-1} (ν_1) provides a fingerprint for hemihydrate.[39] Characterization of the precipitates present at intermediate times showed that the transformation from hemihydrate to gypsum occurs rapidly, and that the sample is almost entirely gypsum after 10 min (Figure S3, Supporting Information).

The effects of confinement on calcium sulfate precipitation were investigated using a simple device, based on the surface force apparatus.[12] Our crossed-cylinder apparatus generates an annular wedge between two half cylinders in which the calcium sulfate is precipitated, and the separation of the cylinders ranges continuously from zero to the macroscale.[40,41] Precipitation of $CaSO_4$ in this apparatus demonstrated that confinement had a marked effect on the morphologies, sizes and polymorphs of the particles, according to their radial distance from the contact point (*DCP*) of the half-cylinders. Precipitates were analysed using SEM and TEM, where insertion of a TEM grid between the half-cylinders at the contact point enabled characterization of small particles, providing vital information about polymorph from electron diffraction. A low-magnification image of a TEM grid placed between the cylinders after 1 h reaction time is shown in **Figure 2**, where the contact point is identified by a region devoid of precipitates and damage to the coated TEM grid surface. Placing a TEM grid between the cylinders

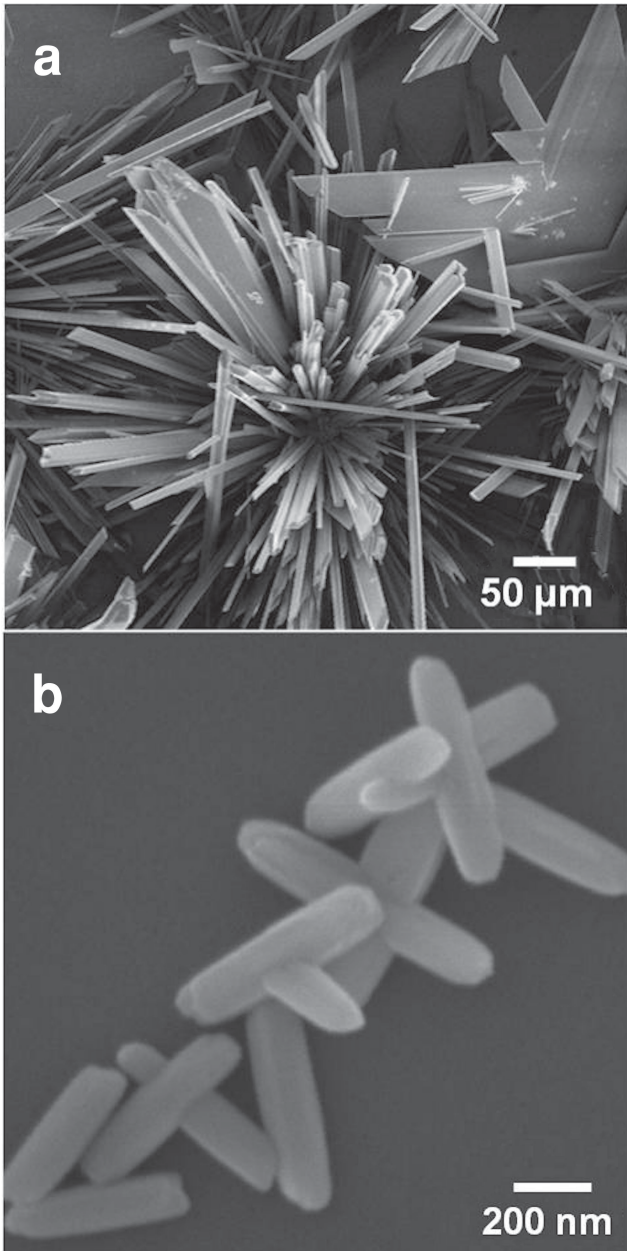

Figure 1. SEM images of $CaSO_4$ particles precipitated from 100 mM solution in the bulk a) after 1 h as gypsum and b) after 1 min as calcium sulfate hemihydrate.

obviously alters the confining volume, such that the surface separation (*SS*) corresponding to a given *DCP* is now half that when the grid is absent. As it is impossible to guarantee that the plane of the TEM grid is perfectly parallel to the cylinder axes, there may be some error in the precise surface separations (although not the trends) quoted. However, at a given surface separation similar particles were precipitated on the TEM grid and on the surfaces of the half cylinders, confirming the validity of this approach (Figure S4, Supporting Information).

When the *DCP* was greater than 350 μm, corresponding to *SS* > 5 μm, the crystals grew as bunches of micron-size,

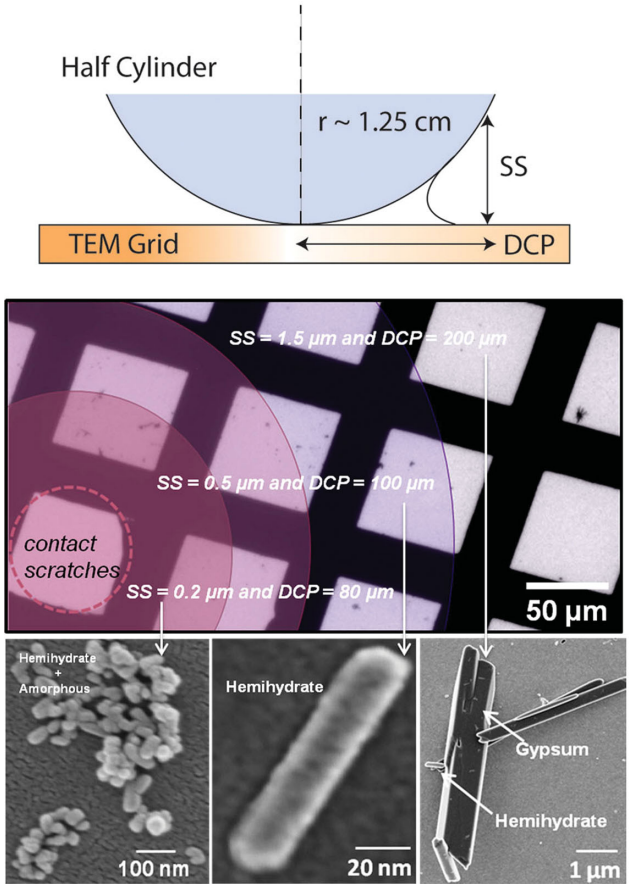

Figure 2. Schematic image of crossed cylinder apparatus, together with a low magnification image of a TEM grid supporting calcium sulfate particles precipitated in confinement, showing the contact point, and the characteristic precipitates generated at different distances from the contact point (*DCP*), corresponding to surface separations (*SS*).

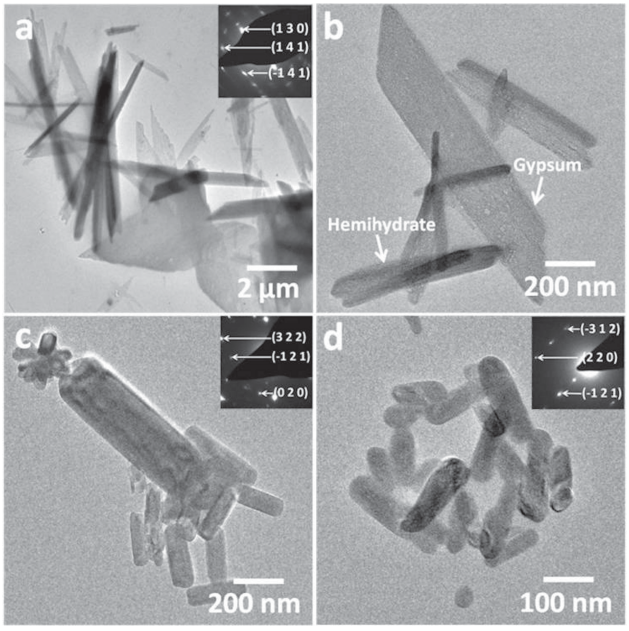

Figure 3. TEM images and corresponding electron diffraction patterns (insets) of calcium sulfate crystals precipitated after 1 h on a TEM grid inserted between the crossed cylinders. The surface separations are approximately a) 5 μm (particles shown are gypsum), b) 1.5 μm (particles shown are a mixture of gypsum and hemihydrate), c) 1 μm (particles shown are hemihydrate with larger hemihydrate rods, more than 500 nm in length), and d) 0.5 μm (particles shown are hemihydrate).

intergrown needles, together with some plate-like particles (**Figure 3**a) which were confirmed as gypsum using electron diffraction (Figure 3a, inset). These crystals are thus identical to those produced in bulk solution. Closer to the contact point, at $DCP = 200$ μm and $SS \approx 1.5$ μm, marked changes in the $CaSO_4$ precipitates were observed and the crystals now appeared as 300–600 nm blocky nanorods together with micron-size, well-defined plates, (Figure 3b) in roughly equal amounts. Electron diffraction confirmed that the nanorods are hemihydrate while the plates are gypsum, an analysis which is consistent with the crystal morphologies. Unlike gypsum precipitated in bulk, the gypsum crystals formed at $SS \approx 1.5$ μm are invariably non-aggregated and show very well-defined plate-like morphologies.

Further changes in the precipitates were observed at smaller surface separations. In the region where $SS \approx 1$ μm, only aggregates of hemihydrate nanorods were observed, as confirmed by electron diffraction (Figure 3c). These were principally about 200 nm in length, although some larger rods and aggregates of small rods were also present. As shown in Figure 3d, individual nanorods of hemihydrate formed at surface separations below 0.5 μm. No aggregates were found and the rods were again smaller, with lengths of 100–200 nm. The corresponding SEM images at surface separations from 5 μm to 0.5 μm are shown in Figure S5 (Supporting Information). The edges and faces of the precipitated crystals also became progressively more irregular with increased confinement, as shown in **Figures 4**a and Figure 4b, for $SS \approx 0.2$ μm. In this separation regime, the hemihydrate nanorods were only 50 nm in length, and aggregates of 10-30 nm nanoparticles (Figure 4c) were observed in some areas. Elemental dispersive X-ray (EDX) analysis of confirmed that these contained Ca and S (Figure 4c, inset), and no evidence for crystallinity was found by selected area electron diffraction (Figure 4d). Conclusive evidence that these particles were amorphous $CaSO_4$ (ACS) was obtained by continued exposure to the electron beam, where partial crystallization to gypsum was apparent after 2 min (Figure 4e). We emphasize that these amorphous particles were viewed after 1 h when confined between the crossed cylinders, while this phase could not be found at all in bulk at 100 mM (due to the time taken to isolate precipitates, they could not be isolated before 1 min). Indeed, although ACS has been observed in bulk reaction solutions, this was achieved by analysing precipitates from 15 mM $CaSO_4$ solutions after 1 min, as ACS is stable for longer periods at lower supersaturations.[36]

In nature, and indeed many practical situations, it is commonly observed that crystallization occurs under the effects of both confinement and soluble additives. We therefore performed experiments in which calcium sulfate was precipitated in the presence of poly(acrylic acid) (PAA) or sodium triphosphate, under systematic control of the degree of confinement. As essential control experiments, calcium sulfate was

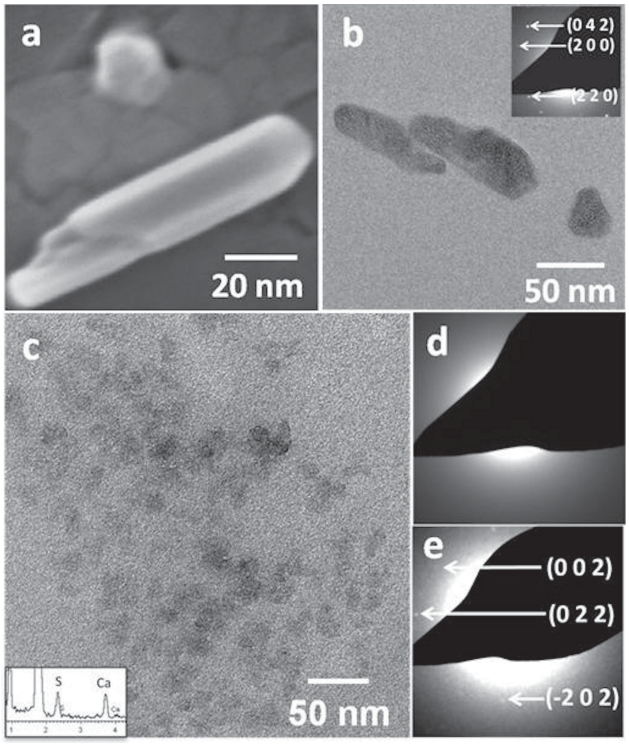

Figure 4. TEM and SEM images of calcium sulfate particles grown at a final concentration of 100 mM in the crossed-cylinder system after 1 h at $SS = 0.2$ μm. In this spatial region, a) SEM and b) TEM images showed hemihydrate nanorods only 50 nm in length, and c) amorphous $CaSO_4$ particles were also observed in this region. The inset in (c) shows the corresponding EDX spectrum, which demonstrates significant Ca and S. d) The selected area electron diffraction pattern of this sample, showing that it is amorphous. e) After 2 min irradiation with the electron beam crystallization to gypsum occurs.

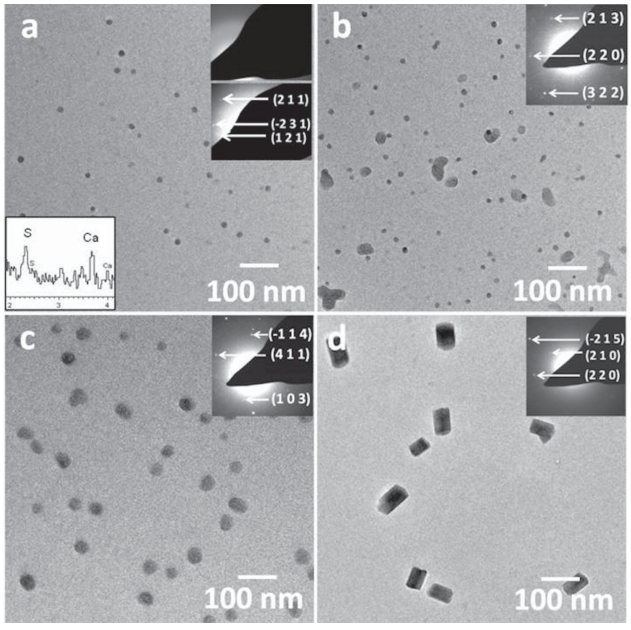

Figure 6. TEM images and corresponding electron diffraction (ED) patterns of calcium sulfate particles precipitated in confinement in the presence of 100 μg/mL PAA at a surface separation of ≈0.5 μm after different incubation times. a) 1 h, showing 20 nm amorphous spheres, together with the corresponding EDX spectrum (inset) showing the presence of Ca and S. The lower inset ED pattern shows crystallization of the amorphous particles to gypsum after heating, b) 5 h, where some amorphous particles have started to transform to hemihydrate, c) 15 h, when hemihydrate nanoparticles are present, and d) after 24 h, showing hemihydrate nanorods.

first precipitated in bulk from a 100 mM solution in the presence of 100 μg/mL PAA or 10 μg/mL sodium triphosphate. As was consistent with previous studies,[42] both additives retarded the crystallization of gypsum so that star-like aggregates of calcium sulfate hemihydrate nanorods were obtained after 1 h, where these were somewhat smaller for the triphosphate (diameter approx 250 nm) than for the PAA (diameter approx 350 nm) (**Figure 5**). These additives therefore effectively inhibit

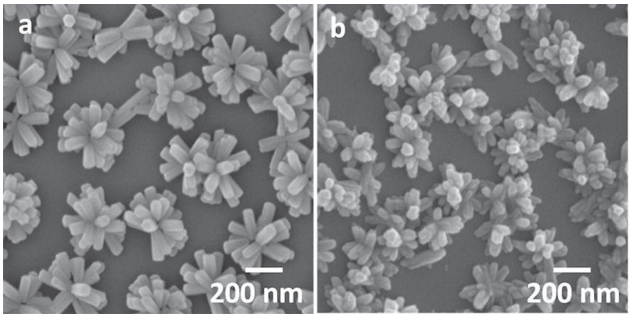

Figure 5. SEM images of $CaSO_4$ particles precipitated from 100 mM solution in bulk after 1 h in the presence of a) 100 μg/mL PAA and b) 10 μg/mL sodium triphosphate.

the recrystallization of hemihydrate to gypsum such that full transformation to gypsum was only achieved after 7 days in the presence of 100 μg/mL PAA, and 5 days in the presence of 10 μg/mL sodium triphosphate. Previous studies with higher concentrations of these additives have also demonstrated that both also retard the transformation of amorphous calcium sulfate to hemihydrate with ACS present at much longer incubation times than in their absence.[42]

Precipitation of $CaSO_4$ in the presence of PAA in confinement resulted in a marked stabilization of its metastable phases. While individual hemihydrate nanorods were found in confinement at $SS = 0.5$ μm after 1 h in the additive-free system, only amorphous nanospheres were observed at the same time and confinement when PAA was present (**Figure 6**a). These particles showed considerable stability, crystallizing only slowly in the apparatus. They also failed to crystallize even after 5 min irradiation in the electron beam in the TEM, and crystallization to gypsum was demonstrated after heating the sample to 200 °C for 10 h. After 5 h reaction time some amorphous nanoparticles had started to crystallize to hemihydrate, generating irregular particles around 20–50 nm in length (Figure 6b). After 15 h, all the spherical nanoparticles had transformed to 50 nm hemihydrate nanocrystals (Figure 6c), which then continued to grow in length to give 100 nm hemihydrate nanorods after 24 h (Figure 6d). In contrast, both gypsum and hemihydrate are found at $SS = 0.5$ μm after 24 h in the absence of PAA,

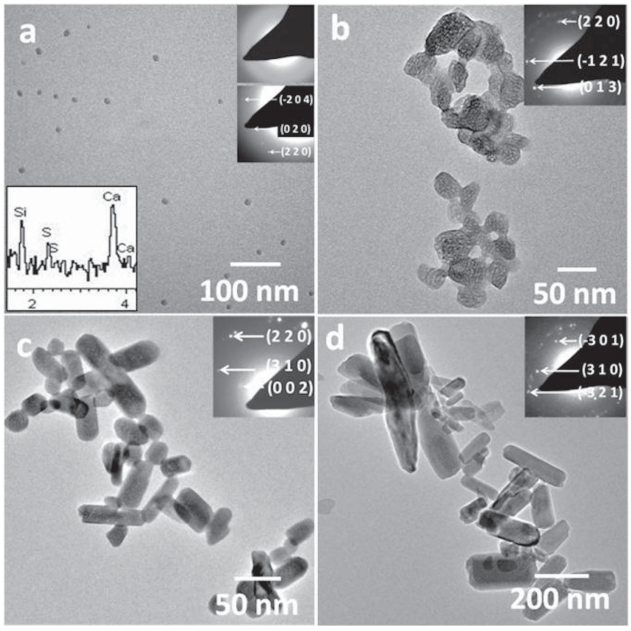

Figure 7. TEM images and corresponding electron diffraction patterns of calcium sulfate particles precipitated in confinement in the presence of 10 μg/mL sodium triphosphate at different surface separations (*SS*) and incubation times. a) *SS* = 0.5 μm, t = 1 h, showing amorphous nanoparticles, together with EDX spectrum (inset) showing the presence of Ca and S. The lower inset ED pattern shows crystallization of the amorphous particles to gypsum after heating. b) *SS* = 0.5 μm, t = 24 h, showing hemihydrate nanoparticles, c) *SS* = 1 μm, t = 1 h, showing hemihydrate nanorods, and d) *SS* = 1 μm, t = 24 h, showing hemihydrate nanorods.

and gypsum started to form in bulk solution in the presence of 100 μg/mL PAA after 24 h.

Sodium triphosphate (10 μg/mL) was also used to compare the effects of a soluble additive on crystallization in confinement with that in bulk solution, and a similar pattern of behavior was observed. Examination of surface separations of 0.5 μm after 1 h clearly showed that the precipitates were 10 nm amorphous nanoparticles (**Figure 7**a), and that they crystallized to 50 nm irregular hemihydrate particles after 24 h (Figure 7b). That confinement plays a key role in offering stabilization was demonstrated by studying larger surface separations of *SS* = 1 μm. This level of confinement was insufficient to stabilize ACS after 1 h reaction time, when well-defined 50–100 nm hemihydrate nanorods were observed (Figure 7c). These continued to grow in size with longer reaction times, but hemihydrate remained the sole phase present after 24 h (Figure 7d). The experiments therefore demonstrate that in combination, confinement and additives can provide considerable stabilization of the metastable polymorphs of calcium sulfate.

4. Discussion

Following a recent surge of interest, it is becoming increasingly clear that calcium sulfate exhibits a complex precipitation behavior. While gypsum is certainly the most stable phase at low temperatures, it was long considered that hemihydrate was only precipitated together with anhydrite from supersaturated, salt-free calcium sulfate solutions at temperatures over 97 °C.[43] This view was called into question following the observation that gypsum can precipitate from solution via amorphous calcium sulfate (ACS) and hemihydrate intermediate phases.[36–38] All demonstrated that the conversion from hemihydrate to gypsum is very slow at low concentrations, and that nanometer-size hemihydrate particles can remain in solution for extended periods. These studies also show that hemihydrate can appear transiently at solution concentrations, which fall below its reported thermodynamic (long-term) solubility.[37] The observed slow conversion from hemihydrate to gypsum is in agreement with many older observations on the very slow kinetics in the $CaSO_4$-H_2O system. Furthermore, the precipitation sequence ACS-hemihydrate-gypsum is entirely in accord with Ostwalds rule of stages in that the metastable phases precipitate first.[44,45]

The experiments performed here demonstrate that confinement can exert a significant influence over calcium sulfate precipitation, leading to a large increase in the lifetime of the metastable phases ACS and hemihydrate. For example, while gypsum was the major product on precipitation from 100 mM bulk solution after just 10 min, particles identical in morphology to those produced in bulk were only observed after 1 h at surface separations (*SS*) of ≈5 μm. With a reduction in the surface separation, changes in the crystal shapes, sizes and polymorphs were also observed. Comparing the reaction products after 1 h at different values of *SS*, a mixture of gypsum and hemihydrate was observed at *SS* ≈ 1.5 μm, where the gypsum particles now appeared as isolated particles rather than the bundles of needles and plates seen in bulk. Hemihydrate was the only phase observed at separations from 0.5 μm to 1 μm, and the particles became smaller as the confinement increased. Note that pure hemihydrate (without traces of gypsum) only persisted for about 1 min after precipitation in bulk 100 mM solution.[36] Finally, at yet smaller separations of 0.2 μm, significant quantities of amorphous calcium sulfate (ACS) were observed in addition to small hemihydrate nanorods after 1 h. Again, it is emphasized that no ACS could be detected in bulk solution after 1 min at these solution concentrations, showing the very significant effect of the confinement.

The efficacy of confinement in controlling calcium sulfate precipitation is further emphasized by reviewing the bulk solution conditions under which ACS and hemihydrate have been observed in other studies. ACS (together with some hemihydrate and gypsum) was only detected after 1 min from a dilute 15 mM solution formed by direct mixing of solutions of $CaCl_2$ and Na_2SO_4,[36] while no ACS was detected at reaction times as early as 10 s in 25 mM solutions.[37] Direct dissolution of hemihydrate to yield solution concentrations of 55 mM was reported to lead to the brief appearance of ACS which then rapidly (within 15–30 s) crystallized to gypsum.[38] The absence of an intermediate hemihydrate phase here is likely due to the higher net $CaSO_4$ concentration and the lack of background electrolyte, which would increase the effective concentration, or activity of $CaSO_4$.

A further striking result from our experiments is that polymorphic control is achieved at separations that are very

large compared to those that usually give rise to confinement effects.[5,13,14] Thus, stabilization of hemihydrate was observed at separations of up to 1 μm, while significant quantities of ACS were noted at separations of 200 nm. In our one previous study using the crossed-cylinder apparatus, we also observed that amorphous calcium carbonate (ACC), the most soluble form of $CaCO_3$, was stabilized with respect to the thermodynamically most stable polymorph calcite at separations in the order of 0.5–1 μm.[29] Notably, no vaterite, which is a common metastable polymorph, was observed. Consideration of the thermodynamics of ACC crystallization in confinement demonstrated that a thermodynamic stabilization of ACC with respect to calcite would only be expected at surface separations of a few nanometers and below, such that the stability was kinetic in origin. Given that the difference in free energy between calcite and ACC is of the same order as that between gypsum and hemihydrate, it is clear that stabilization of hemihydrate at the length scales observed here is not a thermodynamic effect either. The same must be true for ACS, although no quantitative data on its free energy is available in the literature. This therefore contrasts with the precipitation of organic crystals in nanopores, where polymorph selection was attributed to matching of the sizes of the critical nuclei to the pore dimensions.[5]

In bulk solution it has been observed that transformation of hemihydrate occurs via an aggregation-based process, where hemihydrate nanoparticles assemble to give structures which morphologically resemble gypsum, before transforming to gypsum.[37] Experiments in which calcium sulfate was precipitated in the presence of additives have also suggested that hemihydrate may form via an analogous assembly and subsequent crystallization of ACS nanoparticles.[42] These observations are consistent with a growing number of mechanistic studies of the precipitation of insoluble inorganic compounds which suggest that such aggregation-based processes may be widespread.[46,47] Examination of large numbers of the precipitates formed in confinement revealed many particles which comprised aggregates of nanoparticle units, which were comparable to those observed in bulk solution (**Figure 8**). Electron diffraction (Figure 8a inset) and Raman microscopy analysis identified these to be hemihydrate, where the particle in Figure 8a appears to show the transition from ACS to hemihydrate, and Figure 8b the transition from hemihydrate to gypsum.

If the principal mechanisms of hemihydrate and then gypsum formation are aggregation-based, these can be expected to be significantly limited in confinement. Diffusion coefficients are increasingly reduced as confinement increases, such that the diffusion coefficient of a 200 nm spherical particle is only 25% of its bulk value at a separation of 0.5 μm (which approximates to our hemihydrate rods at 0.5 μm surface separation).[48] Further, the diffusion coefficients (D) of 190 nm particles in bulk solution (similar to the particles seen in our experiments) are typically at least two orders of magnitude smaller than the diffusion coefficients of divalent ions.[49] Indeed, hindered diffusion of ions would only begin to become noticeable for surface separations of 20 nm and below,[48] which is an order of magnitude smaller than the smallest separations we study here. Thus, while the confinement levels used here will significantly affect the aggregation of 200 nm particles, the diffusion of ions is totally unaffected.

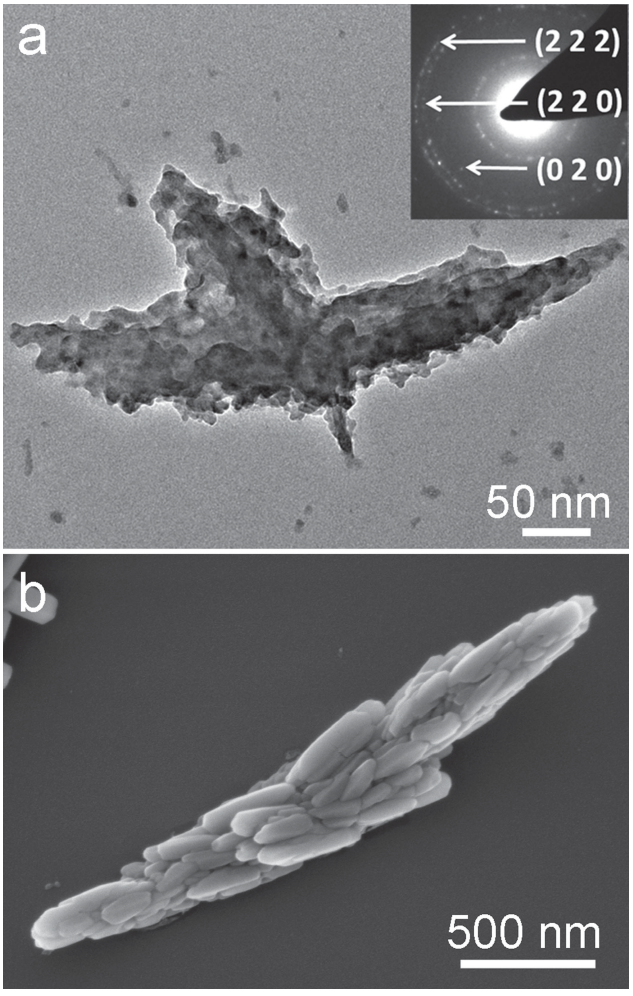

Figure 8. Calcium sulfate particles precipitated in the crossed-cylinder system from a solution of concentration 100 mM after 24 h. a) TEM image and corresponding diffraction pattern of hemihydrate particle precipitated at SS = 0.2 μm and b) SEM image of rod precipitated at SS = 1 μm, comprising an aggregate of hemihydrate nanorods.

An alternative mechanism by which confinement affects precipitation in aqueous solution was proposed in our previous work with calcium carbonate, where it was suggested that stabilization of ACC may derive from the restricted contact between the ACC precipitates and solution in the crossed cylinders apparatus. Crystallization of ACC ($CaCO_3.H_2O$) is accompanied by a dehydration step, and when dry, ACC can be stable for significant periods of time.[50] As the ACC precipitates sandwiched between the surfaces in the crossed cylinders apparatus comprised dense masses of material, several microns wide, at surface separations below ≈1 μm, these deposits would indeed only dehydrate with difficulty; the majority of the surface of the ACC particles would be remote from the interface with water, to which the water of hydration must diffuse for crystallization to occur. Further, a number of studies of the crystallization of ACC in the solid state,[51,52] or with limited contact with water,[32,33] have demonstrated preservation of the form of the original ACC particles in the calcite product, suggesting that

ACC crystallization to calcite does not proceed via an aggregation-based mechanism. Nucleation is less likely to occur in a single small particle (as is produced in confinement), as compared with large ACC particles formed by aggregation in bulk solution. A similar result was obtained for ACC particles precipitated within a microfluidic device, where ACC particles which were stabilized with a coating of poly(aspartic acid) showed remarkable stability at sizes under 100 nm.[31]

The same mechanism cannot be responsible for the stabilization of the metastable calcium sulfate polymorphs in confinement. Transformation of ACS to gypsum ($CaCO_3{\cdot}2H_2O$) via hemihydrate ($CaCO_3{\cdot}0.5H_2O$) also involves changes in the degree of hydration. While the small quantities of ACS precipitated preclude full characterization of this phase, it is clear that ACS must be hydrated as irradiation by the electron beam in the TEM can generate either hemihydrate or gypsum.[36] However, both the ACS and hemihydrate particles appear as either very loose aggregates or isolated particles, as compared with the dense masses of ACC, such that restricted contact with the solution cannot be a factor hindering their conversion. We therefore suggest that stability in confinement can arise from a number of different mechanisms, where restricted contact with the solution, and hindered diffusion and aggregation appear to be important for calcium carbonate ACC and calcium sulfate respectively. Extension of this work to a wider range of materials and further detailed experimental studies of the underlying mechanisms are clearly required to understand fully the role of confinement in controlling crystallization processes.

Finally, we consider the behavior of additives on the crystallization of calcium sulfate in confinement. We have previously demonstrated that additives including poly(acrylic acid) and sodium triphosphate can inhibit the precipitation of calcium phosphate in bulk solution, leading to an increase in the lifetime of the metastable phases ACS and hemihydrate. The behavior of such additives in confinement, however, has not been described, despite its relevance to many processes such as biomineralization, weathering and the formation of nanomaterials. Our results demonstrate that at the length scales employed here (in the order of 1.5 μm to 200 nm), the additives investigated appear to function to a similar level as they do in bulk solution. Thus, combination of confinement and additives confers considerable stability on the metastable calcium sulfate phases, where this effect appears to be equal to a combination of the separate parts, rather than showing evidence of a synergistic effect. This behavior may therefore have relevance to phenomena such as the biomineralization of hemihydrate statoliths (gravity-sensors) in deep-sea medusa,[53,54] whose extended stability is likely due to the combined effects of both soluble additives and confinement.

5. Conclusions

This work provides the first study of the effects of confinement on the precipitation of calcium sulfate and demonstrates a remarkable stabilization of both amorphous calcium sulfate (ACS) and calcium sulfate hemihydrate with respect to gypsum in small volumes. The effect of confinement is attributed to restricted diffusion of precursor particles at small surface separations, thereby hindering aggregation and subsequent conversion to hemihydrate and gypsum. We stress that this is a different mechanism to that invoked to explain the stabilization of amorphous calcium carbonate (ACC) in confinement, showing that confinement effects can operate on many levels. In successfully stabilizing ACS we also demonstrate the value of using confinement as an effective route for identifying new polymorphs and in particular amorphous precursor phases, which may be too short-lived to detect when precipitated from bulk solution. This effect can be significantly enhanced in the presence of additives, which confer considerable additional stability on the metastable intermediate phases. Confinement effects are significant to many natural and technological processes such as the salt-weathering of stone, biomineralization, the templated formation of nanomaterials and even scale formation, which may be promoted by topographical surface defects.[55–57] Understanding the effects of confinement can therefore provide the basis for controlling such phenomena.

Supporting Information

Supporting Information is available from the Wiley Online Library or from the author.

Acknowledgements

The authors thank the EPSRC for financial support via grant EP/H005374/1 (Y.-W.W. and F.C.M.).

Received: March 9, 2013
Revised: April 10, 2013
Published online: June 3, 2013

[1] J. W. Mullin, *Crystallization*, Butterworth-Heinemann, Oxford **2001**.
[2] A. W. Xu, Y. R. Ma, H. Colfen, *J. Mater. Chem.* **2007**, *17*, 415.
[3] A. W. Xu, W. F. Dong, M. Antonietti, H. Colfen, *Adv. Funct. Mater.* **2008**, *18*, 1307.
[4] Y. Y. Kim, K. Ganesan, P. C. Yang, A. N. Kulak, S. Borukhin, S. Pechook, L. Ribeiro, R. Kroger, S. J. Eichhorn, S. P. Armes, B. Pokroy, F. C. Meldrum, *Nat. Mater.* **2011**, *10*, 890.
[5] B. D. Hamilton, J. M. Ha, M. A. Hillmyer, M. D. Ward, *Acc. Chem. Res.* **2012**, *45*, 414.
[6] H. K. Christenson, *J. Phys. Condens. Mater.* **2001**, *13*, R95.
[7] A. E. Charola, J. Puhringer, M. Steiger, *Environ. Geol.* **2007**, *52*, 207.
[8] H. A. Lowenstam, S. Weiner, *On Biomineralization*, Oxford University Press, New York **1989**.
[9] F. C. Meldrum, H. Colfen, *Chem. Rev.* **2008**, *108*, 4332.
[10] E. Beniash, J. Aizenberg, L. Addadi, S. Weiner, *Proc. R. Soc. London Ser. B* **1997**, *264*, 461.
[11] J. Seto, Y. R. Ma, S. A. Davis, F. Meldrum, A. Gourrier, Y. Y. Kim, U. Schilde, M. Sztucki, M. Burghammer, S. Maltsev, C. Jager, H. Colfen, *Proc. Natl. Acad. Sci. USA* **2012**, *109*, 3699.
[12] H. K. Christenson, *Colloid Surf. A* **1997**, *123*, 355.
[13] M. Beiner, G. T. Rengarajan, S. Pankaj, D. Enke, M. Steinhart, *Nano Lett.* **2007**, *7*, 1381.
[14] J. M. Ha, J. H. Wolf, M. A. Hillmyer, M. D. Ward, *J. Am. Chem. Soc.* **2004**, *126*, 3382.
[15] G. T. Rengarajan, D. Enke, M. Steinhart, M. Beiner, *Phys. Chem. Chem. Phys.* **2011**, *13*, 21367.

[16] W. B. Yue, A. N. Kulak, F. C. Meldrum, *J. Mater. Chem.* **2006**, *16*, 408.
[17] B. Wucher, W. Yue, A. N. Kulak, F. C. Meldrum, *Chem. Mater.* **2007**, *19*, 1111.
[18] A. S. Finnemore, M. R. J. Scherer, R. Langford, S. Mahajan, S. Ludwigs, F. C. Meldrum, U. Steiner, *Adv. Mater.* **2009**, *21*, 3928.
[19] D. Yadlovker, S. Berger, *J. Appl. Phys.* **2007**, *101*.
[20] A. Henschel, P. Kumar, T. Hofmann, K. Knorr, P. Huber, *Phys. Rev. E* **2009**, *79*.
[21] B. D. Hamilton, I. Weissbuch, M. Lahav, M. A. Hillmyer, M. D. Ward, *J. Am. Chem. Soc.* **2009**, *131*, 2588.
[22] J. M. Ha, B. D. Hamilton, M. A. Hillmyer, M. D. Ward, *Cryst. Growth Des.* **2012**, *12*, 4494.
[23] P. Horcajada, C. Serre, M. Vallet-Regi, M. Sebban, F. Taulelle, G. Ferey, *Angew. Chem. Int. Ed.* **2006**, *45*, 5974.
[24] G. T. Rengarajan, D. Enke, M. Steinhart, M. Beiner, *J. Mater. Chem.* **2008**, *18*, 2537.
[25] J. M. Ha, B. D. Hamilton, M. A. Hillmyer, M. D. Ward, *Cryst. Growth Des.* **2009**, *9*, 4766.
[26] R. R. Meyer, J. Sloan, R. E. Dunin-Borkowski, A. I. Kirkland, M. C. Novotny, S. R. Bailey, J. L. Hutchison, M. L. H. Green, *Science* **2000**, *289*, 1324.
[27] J. Sloan, A. I. Kirkland, J. L. Hutchison, M. L. H. Green, *Chem. Commun.* **2002**, 1319.
[28] C. J. Stephens, Y.-Y. Kim, S. D. Evans, F. C. Meldrum, H. K. Christenson, *J. Am. Chem. Soc.* **2011**, *133*, 5210.
[29] C. J. Stephens, S. F. Ladden, F. C. Meldrum, H. K. Christenson, *Adv. Funct. Mater.* **2010**, *20*, 2108.
[30] C. C. Tester, R. E. Brock, C.-H. Wu, M. R. Krejci, S. Weigand, D. Joester, *CrystEngComm* **2011**, *13*, 3975.
[31] F. Nudelman, E. Sonmezler, P. H. H. Bomans, G. de With, N. Sommerdijk, *Nanoscale* **2010**, *2*, 2436.
[32] E. Loste, F. C. Meldrum, *Chem. Commun.* **2001**, 901.
[33] E. Loste, R. J. Park, J. Warren, F. C. Meldrum, *Adv. Funct. Mater.* **2004**, *14*, 1211.
[34] H. Orikasa, J. Karoji, K. Matsui, T. Kyotani, *Dalton Trans.* **2007**, 3757.
[35] Y. Y. Kim, N. B. J. Hetherington, E. H. Noel, R. Kroger, J. M. Charnock, H. K. Christenson, F. C. Meldrum, *Angew. Chem. Int. Ed.* **2011**, *50*, 12572.
[36] Y.-W. Wang, Y.-Y. Kim, H. K. Christenson, F. C. Meldrum, *Chem. Commun.* **2012**, *48*, 504.
[37] A. E. S. Van Driessche, L. G. Benning, J. D. Rodriguez-Blanco, M. Ossorio, P. Bots, J. M. Garcia-Ruiz, *Science* **2012**, *336*, 69.
[38] A. Saha, J. Lee, S. M. Pancera, M. F. Braeu, A. Kempter, A. Tripathi, A. Bose, *Langmuir* **2012**, *28*, 11182.
[39] L. P. Sarma, P. S. R. Prasad, N. Ravikumar, *J. Raman Spectrosc.* **1998**, *29*, 851.
[40] T. Kovacs, H. K. Christenson, *Faraday Disc.* **2012**, *159*, 123.
[41] T. Kovacs, F. C. Meldrum, H. K. Christenson, *J. Phys. Chem. Lett.* **2012**, *3*, 1602.
[42] Y.-W. Wang, F. C. Meldrum, *J. Mater. Chem.* **2012**, *22*, 22055.
[43] A. G. Ostroff, *Geochim. Cosmochim. Acta.* **1964**, *28*, 1363.
[44] S. Y. Chung, Y. M. Kim, J. G. Kim, Y. J. Kim, *Nat. Phys.* **2009**, *5*, 68.
[45] P. R. ten Wolde, D. Frenkel, *Phys. Chem. Chem. Phys.* **1999**, *1*, 2191.
[46] J. Baumgartner, A. Dey, P. H. H. Bomans, C. Le Coadou, P. Fratzl, N. A. J. M. Sommerdijk, D. Faivre, *Nat. Mater.* **2013**, *12*, 310.
[47] W. J. E. M. Habraken, J. Tao, L. J. Brylka, H. Friedrich, L. Bertinetti, A. S. Schenk, A. Verch, V. Dmitrovic, P. H. H. Bomans, P. M. Frederik, J. Laven, P. van der Schoot, B. Aichmayer, G. de With, J. J. DeYoreo, N. A. J. M. Sommerdijk, *Nat. Commun.* **2013**, *4*, 1507.
[48] L. Lobry, N. Ostrowsky, *Phys. Rev. B* **1996**, *53*, 12050.
[49] B. M. Belongia, J. C. Baygents, *J. Colloid Interface Sci.* **1997**, *195*, 19.
[50] J. Ihli, A. N. Kulak, F. C. Meldrum, *Chem. Commun.* **2013**, *49*, 3134.
[51] E. H. Noel, Y. Y. Kim, J. M. Charnock, F. C. Meldrum, *CrystEngComm* **2013**, *15*, 697.
[52] J. Ihli, Y.-Y. Kim, E. H. Noel, F. C. Meldrum, *Adv. Funct. Mater.* **2013**, *49*, 3134.
[53] H. Tiemann, I. Sotje, A. Becker, G. Jarms, M. Epple, *Zool. Anz.* **2006**, *245*, 13.
[54] H. Tiemann, I. Sotje, G. Jarms, C. Paulmann, M. Epple, B. Hasse, *J. Chem. Soc. Dalton Trans.* **2002**, 1266.
[55] J. L. Holbrough, J. M. Campbell, F. C. Meldrum, H. K. Christenson, *Cryst. Growth Des.* **2012**, *12*, 750.
[56] N. E. Chayen, E. Saridakis, R. P. Sear, *Proc. Natl. Acad. Sci. USA* **2006**, *103*, 597.
[57] Y. Diao, T. Harada, A. S. Myerson, T. A. Hatton, B. L. Trout, *Nat. Mater.* **2011**, *10*, 867.